Acta Pharmaceutica Sinica B 2024;14(7):3125–3139

Chinese Pharmaceutical Association
Institute of Materia Medica, Chinese Academy of Medical Sciences

Acta Pharmaceutica Sinica B

www.elsevier.com/locate/apsb
www.sciencedirect.com

ORIGINAL ARTICLE

Glycnsisitin A: A promising bicyclic peptide against heart failure that facilitates TFRC-mediated uptake of iron in cardiomyocytes

Jichao Zhou[†], Yuanyuan Liu[†], Xiaoli Wei[†], Meng Yuan[†], Xu Zhang[†], Lingfeng Qin, Bing Cui, Pingping Li, Jing Zhang, Ziming Feng, Jianshuang Jiang, Xiang Yuan, Ruibing Xu, Zhimeng Zhang, Peicheng Zhang[*], Xiaowei Zhang[*], Yanan Yang[*]

State Key Laboratory of Bioactive Substance and Function of Natural Medicines, Institute of Materia Medica, Chinese Academy of Medical Sciences & Peking Union Medical College, Beijing 100050, China

Received 31 October 2023; received in revised form 21 February 2024; accepted 28 February 2024

KEY WORDS

Glycyrrhiza uralensis;
Bicyclic peptides;
Myocardial energy metabolism;
Iron homeostasis;
TFRC

Abstract Zhigancao decoction is a traditional prescription for treating irregular pulse and palpitations in China. As the monarch drug of Zhigancao decoction, the bioactive molecules of licorice against heart diseases remain elusive. We established the HRESIMS-guided method leading to the isolation of three novel bicyclic peptides, glycnsisitins A–C (**1**–**3**), with distinctive C–C and C–O–C side-chain-to-side-chain linkages from the roots of *Glycyrrhiza uralensis* (Licorice). Glycnsisitin A demonstrated stronger cardioprotective activity than glycnsisitins B and C in an *in vitro* model of doxorubicin (DOX)-induced cardiomyocyte injury. Glycnsisitin A treatment not only reduced the mortality of heart failure (HF) mice in a dose-dependent manner but also significantly attenuated DOX-induced cardiac dysfunction and myocardial fibrosis. Gene set enrichment analysis (GSEA) of the differentially expressed genes indicated that the cardioprotective effect of glycnsisitin A was mainly attributed to its ability to maintain iron homeostasis in the myocardium. Mechanistically, glycnsisitin A interacted with transferrin and facilitated its binding to the transferrin receptor (TFRC), which caused increased uptake of iron in cardiomyocytes. These findings highlight the key role of bicyclic peptides as bioactive molecules of Zhigancao decoction for the treatment of HF, and glycnsisitin A constitutes a promising therapeutic agent for the treatment of HF.

*Corresponding authors.
E-mail addresses: pczhang@imm.ac.cn (Peicheng Zhang), zhxw@imm.ac.cn (Xiaowei Zhang), yyn@imm.ac.cn (Yanan Yang).
[†]These authors made equal contributions to this work.
Peer review under the responsibility of Chinese Pharmaceutical Association and Institute of Materia Medica, Chinese Academy of Medical Sciences.

https://doi.org/10.1016/j.apsb.2024.02.026

1. Introduction

As the end-stage consequence of almost all heart diseases, heart failure (HF) is associated with significant morbidity and mortality[1]. Clinically, HF refers to a syndrome in which the structure or function of the heart is impaired due to various causes, leading to an insufficient pumping efficiency that fails to meet the basic metabolic needs of the body[2]. The treatment of HF patients often requires a combination of multiple drugs, such as cardiotonic, diuretic, and vasoconstrictor drugs[3]. However, these symptom relief strategies are insufficient to significantly prolong survival and improve prognosis. Although numerous transcriptional and signaling pathways have been identified in the regulation of pathological HF, there is still a lack of novel effective drug intervention targets for the treatment of HF[4].

Iron is an essential micronutrient in the human body, and its deficiency leads to a myriad of serious consequences[5]. Due to the aberrant expression of hepcidin and frequent gastrointestinal bleeding, patients with HF present a much lower iron content even among those without anemia[6]. As a common comorbidity with HF, iron deficiency significantly increase the mortality of HF patients[7]. In the most recent prevention guidelines from the European Society of Cardiology (ESC), regular testing of iron and hemoglobin content is recommended[3]. Indeed, accumulated studies have noted that supplementation with ferric derisomaltose (FDI) could alleviate HF symptoms and reduce rehospitalization[8,9]. Thus, targeting iron homeostasis is expected to be an effective strategy for treating HF. However, the low absorption rate, gastrointestinal side effects, and risk of iron overload remain the major reasons limiting the widespread application of iron supplements in the treatment of HF. Therefore, the development of novel drugs that improve the specific uptake of iron in cardiomyocytes and minimize adverse effects might be a potential strategy for the treatment of HF.

Zhigancao decoction mentioned in the treatise on febrile diseases (a classic Chinese medical book written by Zhongjing Zhang during the late Eastern Han Dynasty) was the classic formula for treating heart diseases[10]. Given that licorice is the monarch drug in the Zhigancao decoction, it is anticipated to possess bioactive compounds that could contribute to the therapeutic properties for heart diseases. To date, numerous phytochemical studies have been conducted on licorice, resulting in the isolation of triterpenoids, flavonoids, coumarins, and phenolic acids[11−13]. However, the effects of these compounds against HF have not been scientifically established, leaving the active compounds responsible for the cardio-protection of licorice unclear. Hence, it is hypothesized that yet-undiscovered bioactive compounds that hold potential against HF exist in licorice.

In this study, we implemented an HREISMS-guided approach to reduce the redundant isolation of commonly occurring constituents in licorice. As a result, three novel bicyclic peptides glycnsisitins A−C (**1**−**3**) (Supporting Information Fig. S28), featuring distinctive C−C and C−O−C side-chain-to-side-chain linkages were isolated for the first time from the roots of *Glycyrrhiza uralensis*. Among them, glycnsisitin A showed significant potential to enhance the viability of cardiomyocytes and inhibit the production of mitochondrial reactive oxygen species (Mito-ROS) induced by doxorubicin (DOX), a potent chemotherapeutic agent. DOX is known for its dose-dependent and irreversible cardiotoxicity, leading to cardiac dysfunction and HF. Here, a mouse model of DOX-induced HF was employed to assess the cardioprotective effects of glycnsisitin A. Our findings demonstrated, for the first time, that glycnsisitin A exhibits remarkable protective effects against DOX-induced cardiac dysfunction and myocardial injury. Mechanistically, the TFRC-dependent iron homeostasis pathway was involved in the cardioprotective function of glycnsisitin A. By interacting with transferrin, glycnsisitin A increased its binding affinity with transferrin receptor (TFRC) and improved iron content in myocardial tissue of dysfunctional hearts. These results first confirmed that TFRC is a potential therapeutic target of glycnsisitin A for HF treatment. Moreover, our findings unveil the bicyclic peptide as a pivotal bioactive molecule within the Zhigancao decoction for the treatment of HF. The remarkable cardioprotective effects exhibited by glycnsisitin A position it as a promising therapeutic agent for the treatment of HF.

2. Results

2.1. Discovery and identification of glycnsisitins A−C from *Glycyrrhiza uralensis* roots

In the LC−HRESIMS^2 analysis, a unique peptide (*m/z* 967.4191) whose fragmentations included typical tyrosine (136.0755 Da), valine (72.0816 Da), and proline (70.0660 Da) iminium ions was discovered (Fig. 1). To identify its structure, targeted phytochemistry research was carried out. As a result, glycnsisitin A (**1**) was successfully isolated with 30.0 g. Its molecular formula was inferred as $C_{49}H_{58}O_{13}N_8$ by HRESIMS data at *m/z* 967.4191 ([M + H]$^+$, calcd. for $C_{49}H_{59}O_{13}N_8^+$, 967.4196). The IR spectrum vibrational peaks at 3313, 1665, 1513, and 1460 cm^{-1} suggested the presence of hydroxyl, carbonyl, and phenyl groups. The ^{13}C NMR spectrum presented nine carbonyl carbons and eight typical α-amino acid carbons, which suggested the presence of eight amino acid residues in compound **1**. The ^{1}H NMR spectrum of **1** assigned three benzene rings including one ABX system and two AA′BB′ systems. According to the HMBC correlations from α-H (δ_H 6.12) of Gly^4 to C-2 (δ_C 130.4)/C-4 (δ_C 154.9) in Tyr^8, a C−C nonpeptide bond between Tyr^8 and Gly^4 was confirmed. Apart from eight carbonyl carbons of amino acid residues, another carbonyl carbon (δ_C 176.3) was assigned to a pyroglutamic acid residue. Because C-γ (δ_C 75.4) was obviously shifted downfield, C-γ was an oxygenated methine. Furthermore, the HMBC correlations from H-γ (δ_H 5.10) of Pyroglu^1 to C-4 (δ_C 154.7) of Tyr^6 confirmed the presence of a C−O−C nonpeptide bond between them. In addition, 163.0870 and 209.0922 Da ions also indicated the presence of nonpeptide bond connections (Fig. 1). Finally, eight characteristic amino acid residues were presented as Tyr (3 ×), Val (2 ×), Gly, Pro, and PyroGlu by careful analysis of NMR spectra (Supporting Information Figs. S1−S6). The restrictions of the molecular formula and the corresponding degrees

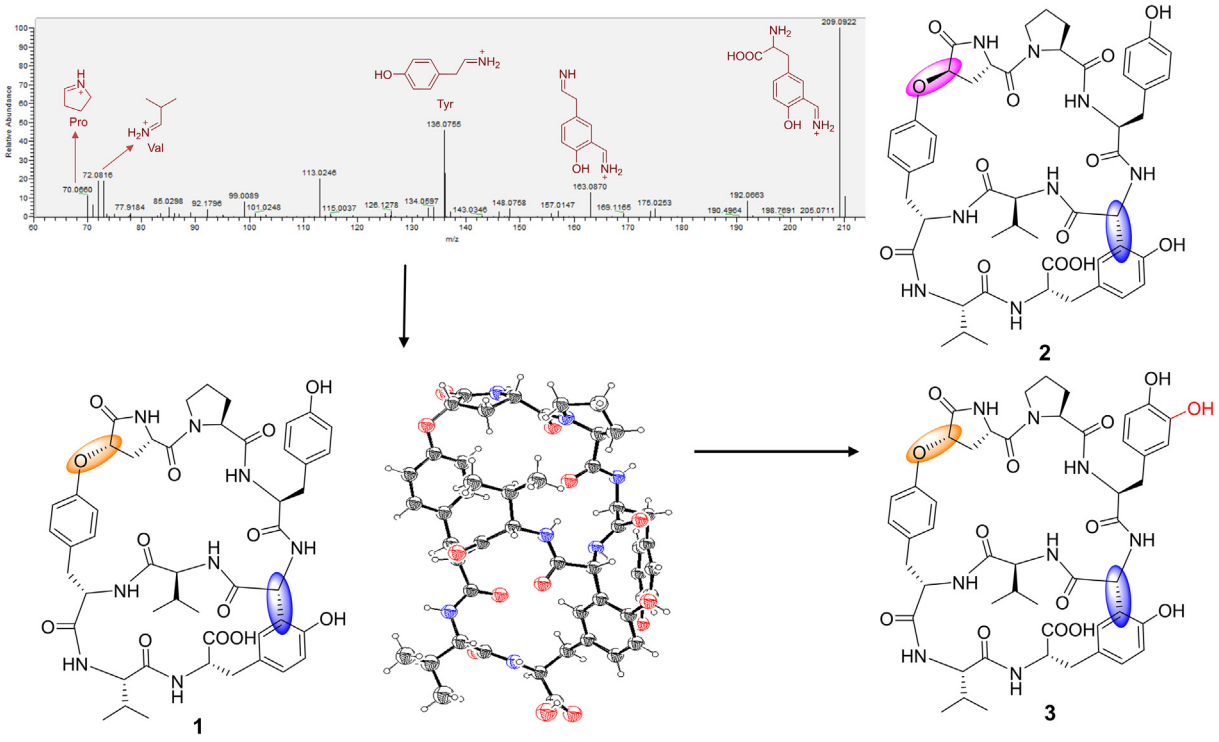

Figure 1 Chemical structures of **1**−**3** and X-ray crystal structure of **1**.

of unsaturation indicated that **1** was a cyclopeptide. The sequence of amino acid residues was established by deep analysis of HMBC and ROESY spectra. The absolute configurations of Val[7], Val[5], Tyr[3], and Pro[2] were determined to L through Marfey's method (Supporting Information Fig. S31). Only the absolute configurations of chiral carbons at nonpeptide bond junctions must be determined. In the ROESY spectrum, the correlation of H-α and H-γ in Pyroglu[1] illustrated that the absolute configuration of C-γ was *S*. The absolute configuration of C-α in Gly[4] was determined to be *R* through comparison of ROESY correlations with optimized conformations at the B3LYP/6-31G(d) level[14] (Fig. 2 and Supporting Information Fig. S29). Fortunately, this deduction was substantiated by single-crystal X-ray diffraction (Fig. 1). Therefore, the structure of **1** was established as a bicyclic peptide and named glycnsisitin A.

Glycnsisitin B possessed the same molecular formula of $C_{49}H_{58}O_{13}N_8$ as glycnsisitin A through the HRESIMS data at *m/z* 967.4191 ($[M + H]^+$, calcd. for $C_{49}H_{59}O_{13}N_8^+$, 967.4196). The NMR data (Supporting Information Figs. S10−S15) suggested the same planar structures of them. However, the chemical shifts of PyroGlu[1] residue were significantly shifted to downfield comparing with same carbons of glycnsisitin A in the ^{13}C NMR spectrum. This suggested the absolute configurations of PyroGlu[1] residue were different from glycnsisitin A. For the absolute configuration of natural PyroGlu was L, only the absolute configuration of C-γ has changed. In the ROESY spectrum, the key correlation of H-α and H-γ in Pyroglu[1] was not observed, which indicated the relative configuration of these two protons was *trans*. Therefore, the absolute configuration of C-γ was determined to be *R*. In addition, the absolute configuration of C-α in Gly[4] was established as *R* according to the consistent ROESY correlations of H-α with glycnsisitin A. This was also confirmed by Marfey's method (Supporting Information Figs. S32, S34, and S35). Finally, the structure of glycnsisitin B was confirmed as shown in Fig. 1.

Glycnsisitin C was isolated as white amorphous powder. Compared with glycnsisitin A, an additional hydroxyl was observed in glycnsisitin C through HRESIMS data (*m/z* 983.4139, $[M + H]^+$, calcd. for $C_{49}H_{59}O_{14}N_8^+$, 983.4145). This was also confirmed by the NMR spectra (Supporting Information Figs. S19−S24). In the ^1H NMR spectrum of glycnsisitin C, two ABX systems and one AA′BB′ system were presented that was different from glycnsisitin A. This suggested that the additional hydroxyl was attached to one of the benzene rings. The HMBC correlation from H-5 (δ_H 6.48) of Tyr[3] to C-3 (δ_C 145.6) of Tyr[3] indicated this hydroxyl was attached at the C-3 of Tyr[3]. Besides, the identical peptide sequences with glycnsisitin A were determined by analysis of the spectroscopic data of glycnsisitin C. The absolute configurations of two chiral carbons at nonpeptide bond junction were determined to *R* (C-α in Gly[4]) and *S* (C-γ in PyroGlu[1]) by the same method as glycnsisitin A through ROESY correlations with optimized conformations at B3LYP/6-31G(d) level (Supporting Information Fig. S30) and Marfey's method (Supporting Information Figs. S33−S35). Ultimately, the structure of glycnsisitin C was verified.

2.2. *Glycnsisitin A protects cardiomyocytes from DOX-induced cell death and mitochondrial ROS accumulation*

To test whether glycnsisitins A−C (**1**−**3**) possess cardioprotective potential, we performed a cell viability assay in H9C2 cardiomyocytes and found that all these bicyclic peptides could significantly improve cell viability upon DOX treatment (Fig. 3a). The EC_{50} of glycnsisitins A (GL-A), B (GL-B), and C (GL-C) were determined to be 1.456, 6.730, and 3.735 μmol/L, respectively (Fig. 3b−d). Further investigations using *ex vivo* cultured

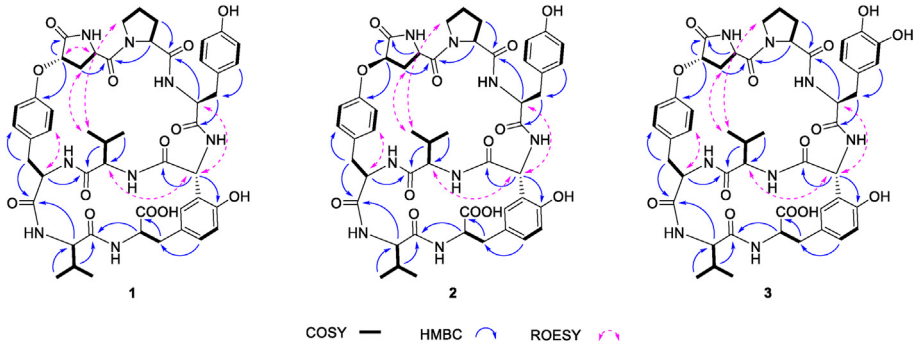

Figure 2 Key HMBC, $^{1}H-^{1}H$ COSY, and ROESY correlations of **1**–**3**.

primary cardiomyocytes were focused on glycnsisitin A. Compared with the solvent control group, exposure of cardiomyocytes to 8.6 μmol/L DOX for 24 h resulted in an approximately fourfold increase in the number of trypan blue-positive cells. However, the presence of glycnsisitin A significantly attenuated the cardiotoxicity induced by DOX and reduced cell death (Fig. 3e). In parallel, the cell survival assay results also proved the primary cell protective function of glycnsisitin A (Fig. 3f). Additionally, the introduction of DOX to cardiomyocytes led to an elevation in the release of lactate dehydrogenase (LDH), an enzyme indicative of cellular damage, which could be significantly suppressed upon glycnsisitin A treatment (Fig. 3g). Given that ATP serves as the primary energy currency in cellular metabolism, particularly in energy-demanding processes within cardiomyocytes, we measured total ATP contents to evaluate cell respiration capacity and mitochondrial function. Although glycnsisitin A treatment did not have an impact on ATP levels in cardiomyocytes under normal conditions, a substantial difference was observed in the presence or absence of glycnsisitin A following DOX induction (Fig. 3h), highlighting the indirect

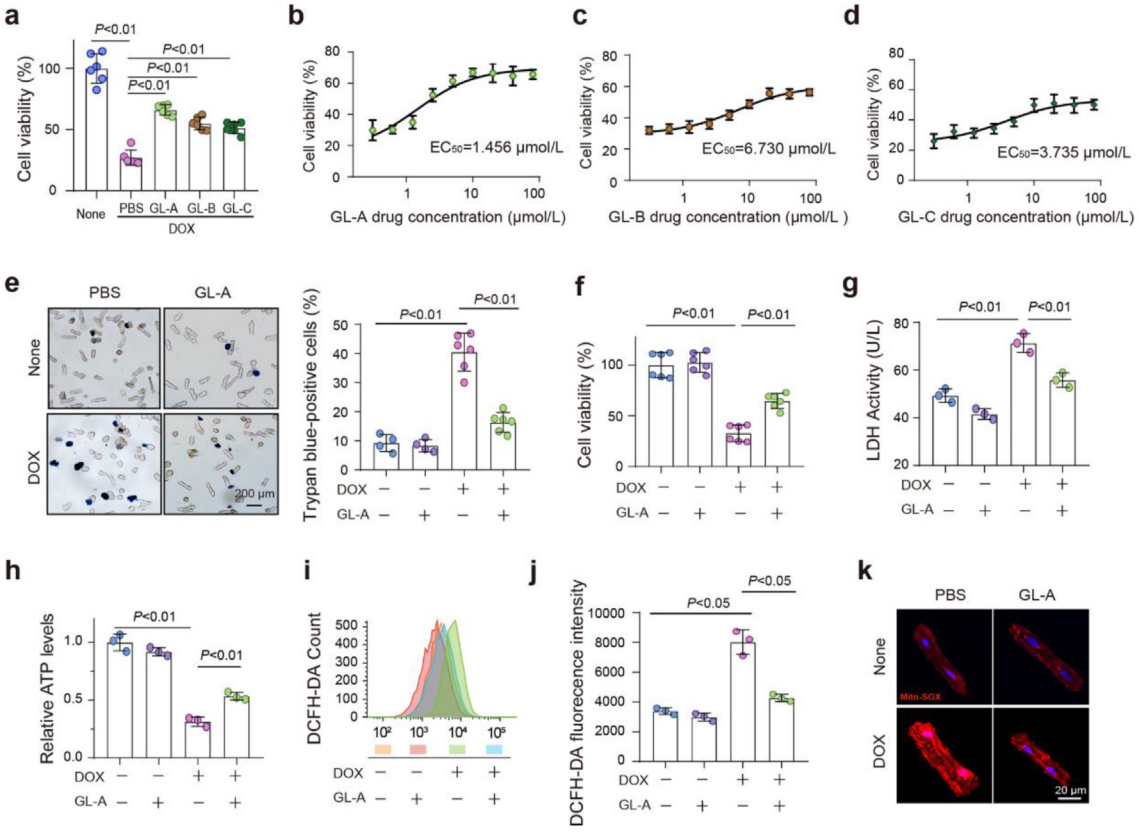

Figure 3 Glycnsisitin A protects against DOX-induced cardiotoxicity and ROS production. (a) Alamar blue assay was used to quantitatively analyze the relative cell viability of DOX-injured H9C2 cells treated with glycnsisitins A–C (**1**–**3**). (b–d) The calculated EC_{50} values for glycnsisitins A, B, and C. (e) Representative images of primary adult rat cardiomyocytes stained with trypan blue, and quantitative analysis was performed to determine the number of trypan blue-positive cells (indicating dead cells). (f) Alamar blue assay was conducted on DOX-injured primary cardiomyocytes treated with glycnsisitin A. (g, h) The LDH activity and relative ATP levels of primary cardiomyocytes. (i, j) ROS levels in primary cardiomyocytes detected by flow cytometry with DCFH-DA staining. (k) Representative images of primary cardiomyocytes were captured to characterize the generation of mitochondrial ROS by MitoSox fluorescence staining. The data are presented as the mean ± SEM.

cardiotonic effect of glycnsisitin A. Since the accumulation of intracellular ROS is a significant contributor to necroptosis during DOX-induced myocardial injury, total ROS accumulation in cardiomyocytes was assessed by DCFH-DA staining. We observed that the levels of ROS in cardiomyocytes were dramatically increased following treatment with DOX, which could be turned over by glycnsisitin A (Fig. 3i and j). Furthermore, we examined the generation of reactive oxygen species (ROS) specifically within the mitochondria using MitoSOX staining and found that glycnsisitin A significantly attenuated the excessive generation of mitochondrial ROS induced by DOX (Fig. 3k). These findings confirm that glycnsisitin A provides protection to cardiomyocytes against cell injury and oxidative stress induced by DOX.

2.3. *Glycnsisitin A ameliorates DOX-induced cardiac dysfunction and remodeling*

To confirm our *in vitro* findings, we established an acute DOX-induced HF mouse model to evaluate whether glycnsisitin A could enhance cardiac systolic function and increase mouse survival. Indeed, mice subjected to intraperitoneal injection of 15 mg/kg DOX exhibited a 50% mortality rate. However, the survival rate of mice intraperitoneally treated with glycnsisitin A increased in a dose-dependent manner, with the highest dosage (200 mg/kg) demonstrating an overall survival rate of 90% compared to the control group (Fig. 4a). Both cedilanid and glycnsisitin A (100 mg/kg) treatment resulted in a higher LV ejection fraction (EF, Fig. 4b and c) and fractional shortening (FS, Fig. 4d), as well as reduced LV internal dimension diameter (LVIDd, Fig. 4e). Moreover, glycnsisitin A demonstrated therapeutic superiority to cedilanid in myocardial remodeling, as evidenced by a thicker diastolic LV anterior wall diameter (LVAWd, Fig. 4f), lesser collagen deposition (Fig. 4g and h) and lower pathology score (Fig. 4i and j). The protective effects of glycnsisitin A against myocardial injury were verified by detecting serum CK and LDH activity, which are the primary predictive and diagnostic markers in HF. As expected, the activity of the LDH and CK enzymes markedly increased in DOX-induced HF mice, which could be completely reversed by glycnsisitin A (Fig. 4k and l). In addition, glycnsisitin A treated mice had lower levels of brain-type natriuretic peptide (BNP) and N-terminal pro-brain natriuretic peptide (NT-proBNP) in plasma as compared to DOX-induced HF mice, indicating an alleviated myocardial damage (Fig. 4m and n). These data provide strong *in vivo* evidence for the protective effects of glycnsisitin A against cardiac dysfunction and remodeling.

2.4. *Glycnsisitin A attenuates DOX-induced HF by maintaining myocardial iron homeostasis*

To explore the mechanism underlying the protective role of glycnsisitin A against DOX-induced cardiotoxicity, RNA sequencing (RNA-Seq) analysis was performed to screen differentially expressed genes, followed by gene functional analysis to identify potential functional targets. We found that glycnsisitin A treatment led to 1842 genes whose expression changed $\geq$1.3-fold in healthy mouse heart tissue, while the number increased to 2258 genes under HF conditions, which is most likely caused by the global change in gene expression (3045 genes) upon DOX treatment (Fig. 5a). Venn diagrams were generated to further explore the relationships among the distinct sets of differentially expressed genes (DEGs) (Fig. 5b). KEGG pathway analysis of these DEGs indicated that HF-related gene sets, such as hypertrophic cardiomyopathy (HCM), dilated cardiomyopathy (DCM), and arrhythmogenic right ventricular cardiomyopathy (ARVC), were most enriched in the glycnsisitin A plus DOX cotreatment group compared with the DOX group, implying the protective role of glycnsisitin A against myocardial dysfunction at the gene expression level. In addition, several biological process (BP) gene sets, such as folate biosynthesis and mineral absorption, also drew our attention (Fig. 5c). To prevent the loss of significant information due to inappropriate fold change and *P*-value threshold definitions, we performed GSEA by sorting the entire ranked gene list based on significant differences. Following glycnsisitin A treatment, the gene sets related to iron metabolism, such as iron homeostasis and iron transport, exhibited the highest levels of enrichment (Fig. 5d). Consequently, a heatmap was derived using the FPKM values of the enriched gene sets to visually illustrate the variations among the specified groups (Fig. 5e). Collectively, these findings indicate that iron homeostasis might be involved in the cardioprotective function of glycnsisitin A.

2.5. *Glycnsisitin A increases the myocardial iron content by enhancing the binding ability of transferrin with TFRC*

To verify the iron metabolism regulatory activity of glycnsisitin A, molecular docking was utilized to estimate the binding capacity between glycnsisitin A and proteins associated with iron homeostasis. The results showed a significant binding affinity (−9.3 kcal/mol) between glycnsisitin A and transferrin (Fig. 6a). As shown in Supporting Information Fig. S36, glycnsisitin A-bonding by transferrin involved hydrogen bonding, alkyl, salt bridge, and Pi-sigma interactions. Additionally, the molecular docking study between glycnsisitin A and TFRC was also performed. The results showed −8.9 kcal/mol binding affinity and revealed that hydrogen bonds were formed between glycnsisitin A and amino acid residues (Supporting Information Fig. S37). Furthermore, during the surface plasmon resonance (SPR) analysis, glycnsisitin A showed a pretty strong response signal on transferrin-coated CM5 sensor chips ($K_D = 2.415 \times 10^{-6}$ mol/L), indicating the direct physical interaction between compound and protein target (Fig. 6b). Given that both transferrin and TFRC play crucial roles in the transportation of iron into cells for storage and subsequent utilization, the iron content in the myocardium was further measured to verify the regulatory function of glycnsisitin A. As expected, a significant loss of iron was observed following DOX treatment, but the iron levels could be effectively restored to normal by glycnsisitin A (Fig. 6c). Immunoblotting was conducted to determine the relative abundance of transferrin and TFRC in heart tissues, and the statistical analysis revealed a significant decrease in transferrin expression by over 50% in the heart tissues of DOX-treated mice. However, regardless of the presence of DOX, glycnsisitin A significantly increased the total transferrin levels in the mouse myocardium, which is consistent with the trend observed for TFRC (Fig. 6d and e). Transferrin is a 76-kDa glycoprotein that is mainly produced in the liver, which carries iron in the circulation. In this context, the protein level of transferrin in the heart can be affected both by the transcription level and the uptake ratio of serum transferrin. To address this concern, we determined the relative mRNA level of cultured cardiomyocytes and found that glycnsisitin A did not affect the mRNA content of transferrin but increased the TFRC transcription (Fig. 6f). In order to deduce the possible mechanisms behind the observed increase in TFRC mRNA level, we used CHX to inhibit protein synthesis (Fig. 6g)

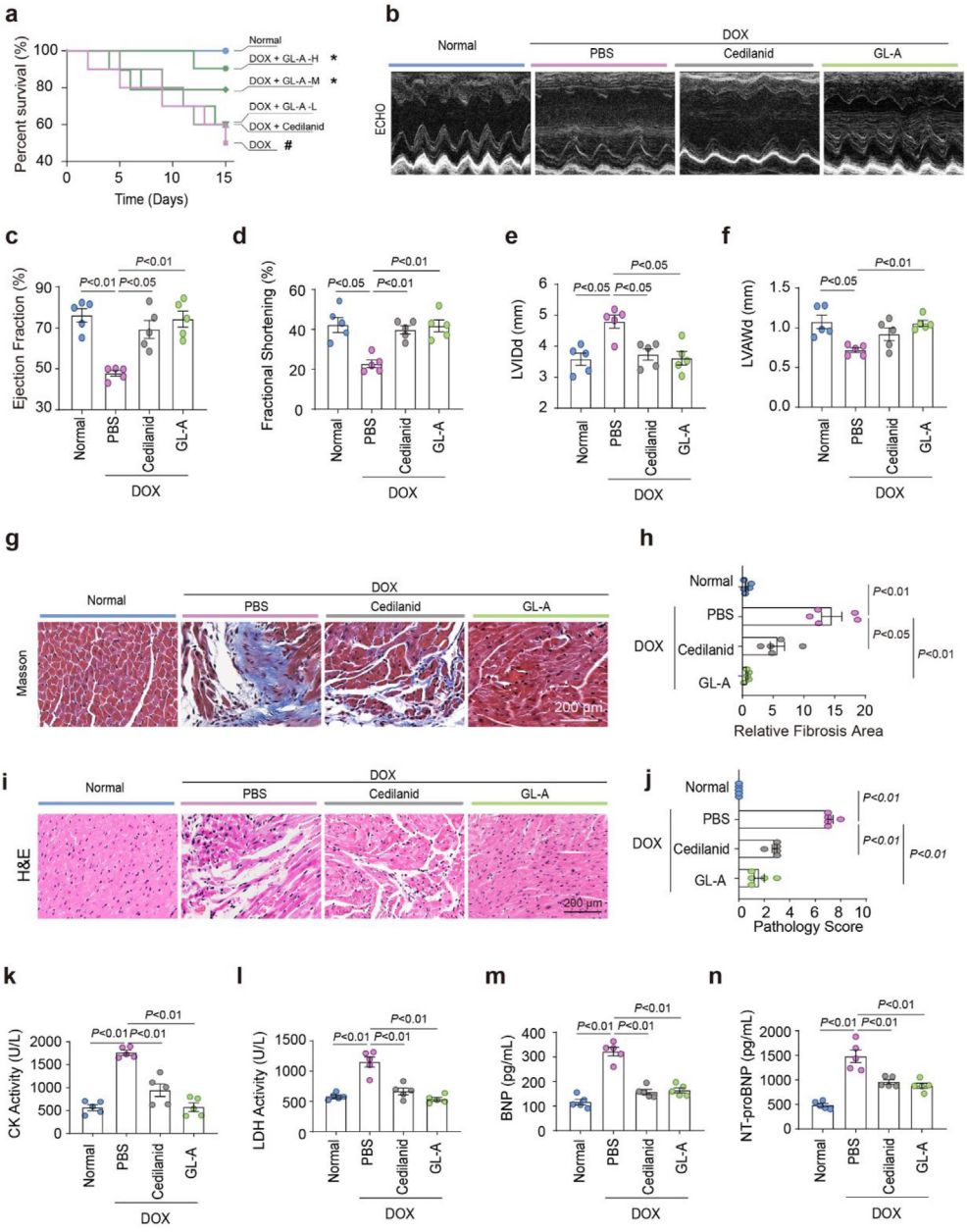

Figure 4 Glycnsisitin A attenuates DOX-triggered cardiac systolic dysfunction and myocardium fibrosis. (a) Kaplan−Meier survival curves were generated for mice treated with PBS, glycnsisitin A, or cedilanid following the induction of an acute HF model. $^{\#}P < 0.05$, compared with normal group; $^{*}P < 0.05$, compared with the DOX group. (b) Representative images of left ventricular (LV) M-mode echocardiograms. (c) LV ejection fraction (EF), (d) Left ventricular fractional shortening (FS), (e) internal dimension diameter (LVIDd), and (f) anterior wall diameter (LVAWd) were calculated by echocardiographic analysis. (g, h) Representative Masson trichrome staining images of heart tissue and quantification of relative fibrosis area. (i, j) Representative hematoxylin-eosin (H&E) staining images of heart tissue and quantitative analysis of myocardial histopathological scores. (k) Creatine kinase (CK) and (l) lactate dehydrogenase (LDH) activity in mouse serum. (m) Brain-type natriuretic peptide (BNP) and (n) N-terminal pro-brain natriuretic peptide (NT-proBNP) content in mouse serum. The data are presented as the mean ± SEM.

and found that glycnsisitin A could increase the half-life of transferrin protein (Fig. 6h) but decreased TFRC stability (Fig. 6i), which may be the consequence of increased clathrin-mediated endocytosis and reduced endosome recycling. Subsequently, we performed a cellular immunoprecipitation and found that the content of immunoprecipitated transferrin is much higher in glycnsisitin A treated group, suggesting that glycnsisitin A could increase the protein−protein interaction between transferrin and TFRC (Fig. 6j). Moreover, the truncated recombinant TFRC-His (residues 88−760) protein expressed in bacteria were purified using Ni-NAT affinity chromatography (Fig. 6k). By coating transferrin onto the surface of a 96-well plate, we detected the relative change in captured TFRC-His proteins caused by glycnsisitin A according to the absorption intensity of the indicated different groups. Glycnsisitin A saturated transferrin binds much more TFRC than the negative control group, thereby

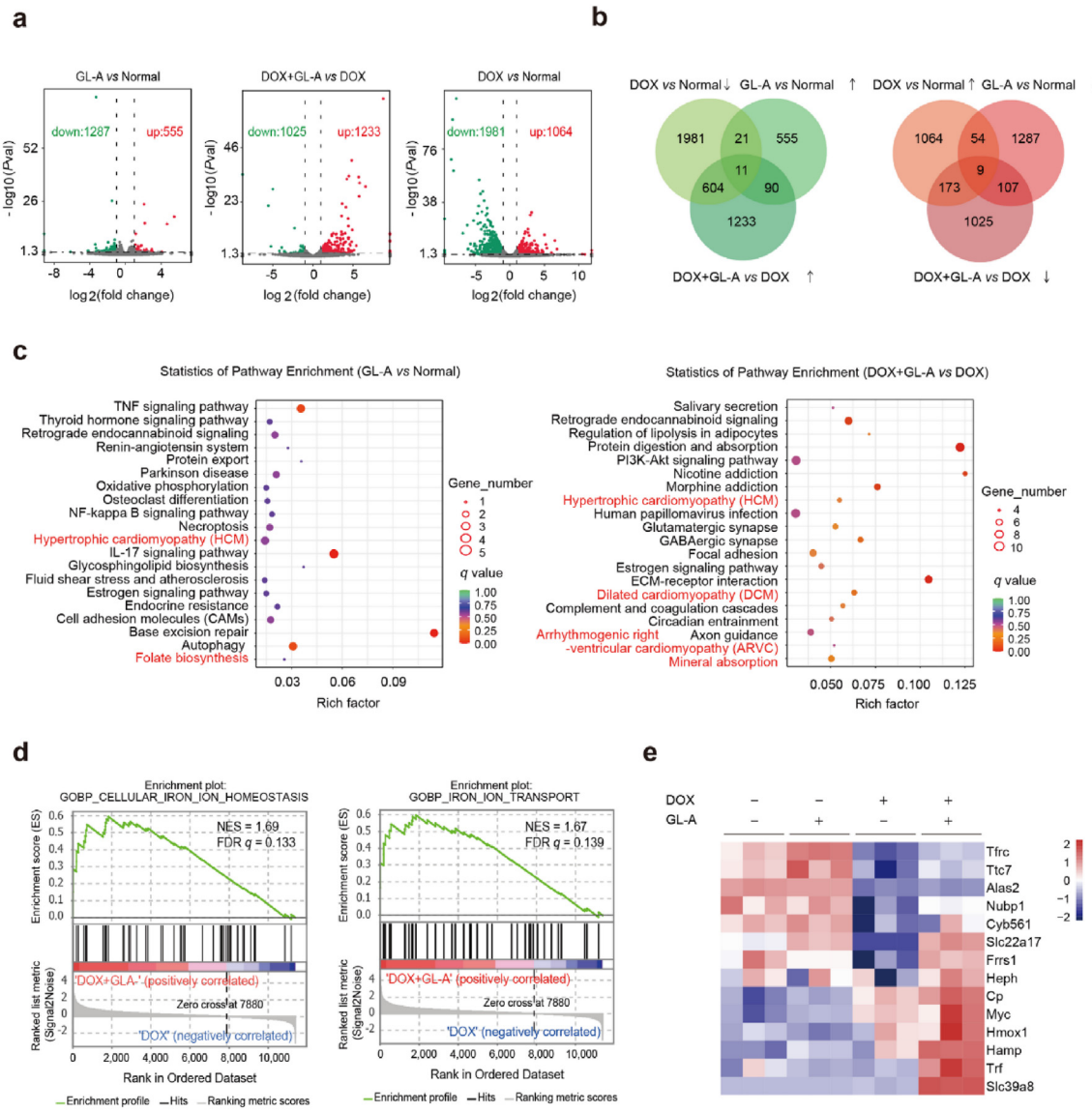

Figure 5 Glycnsisitin A attenuates DOX-induced HF by maintaining myocardial iron homeostasis. (a) Using RNA-Seq analysis, volcano plots were generated to visualize the differentially expressed genes (DEGs) in heart tissues when comparing glycnsisitin A *vs*. Normal, DOX + glycnsisitin A *vs*. DOX, and DOX *vs*. Normal conditions. Red: upregulated genes; Green: downregulated genes; gray: no DEGs. $n = 3$ per group. (b) A Venn diagram was constructed to illustrate the shared DEGs among various sets. (c) KEGG pathway bubble diagrams were generated to visualize the enrichment of biological pathways in the comparisons of glycnsisitin A *vs.* normal and DOX + glycnsisitin A *vs*. DOX. The abscissa is the rich factor (sample number/background number), and the ordinate is the KEGG enrichment pathway. Bubble size indicates the number of differentially enriched genes, and bubble color indicates the *P*-value of enrichment significance. (d) GSEA plots of the iron metabolism-related gene modules in the myocardium of mice following treatment with DOX or glycnsisitin A and DOX. NES, normalized enrichment score; FDR q, false discovery rate. (e) Heatmap displaying the expression of iron homeostasis-related genes in the four indicated groups.

demonstrating its capacity to enhance ligand and receptor affinity (Fig. 6l). Taken together, these data suggest that glycnsisitin A is an exceptionally effective iron metabolism-regulating compound that can activate transferrin and significantly enhance its binding affinity with TFRC.

2.6. *Functional antagonism of TFRC eliminates the cardioprotective effects of glycnsisitin A both in vitro and in vivo*

To further validate whether the cardioprotective effects of glycnsisitin A are exerted in a TFRC-dependent manner, we applied a TFRC neutralizing antibody (NAb-anti-TFRC) to block the normal iron transport process of primary cardiomyocytes. Consistent with our *in vivo* findings, glycnsisitin A restored the decline in iron content within DOX-treated cardiomyocytes, which was completely abolished when cardiomyocytes were pretreated with NAb-anti-TFRC (Fig. 7a). Given the sharp variation in the cellular iron content, it is worth investigating whether NAb-anti-TFRC could impact the ability of glycnsisitin A to enhance cardiomyocyte viability. We found that neutralizing TFRC led to a higher ratio of cell death compared to treatment with DOX and glycnsisitin A (Fig. 7b). Additionally, the LDH

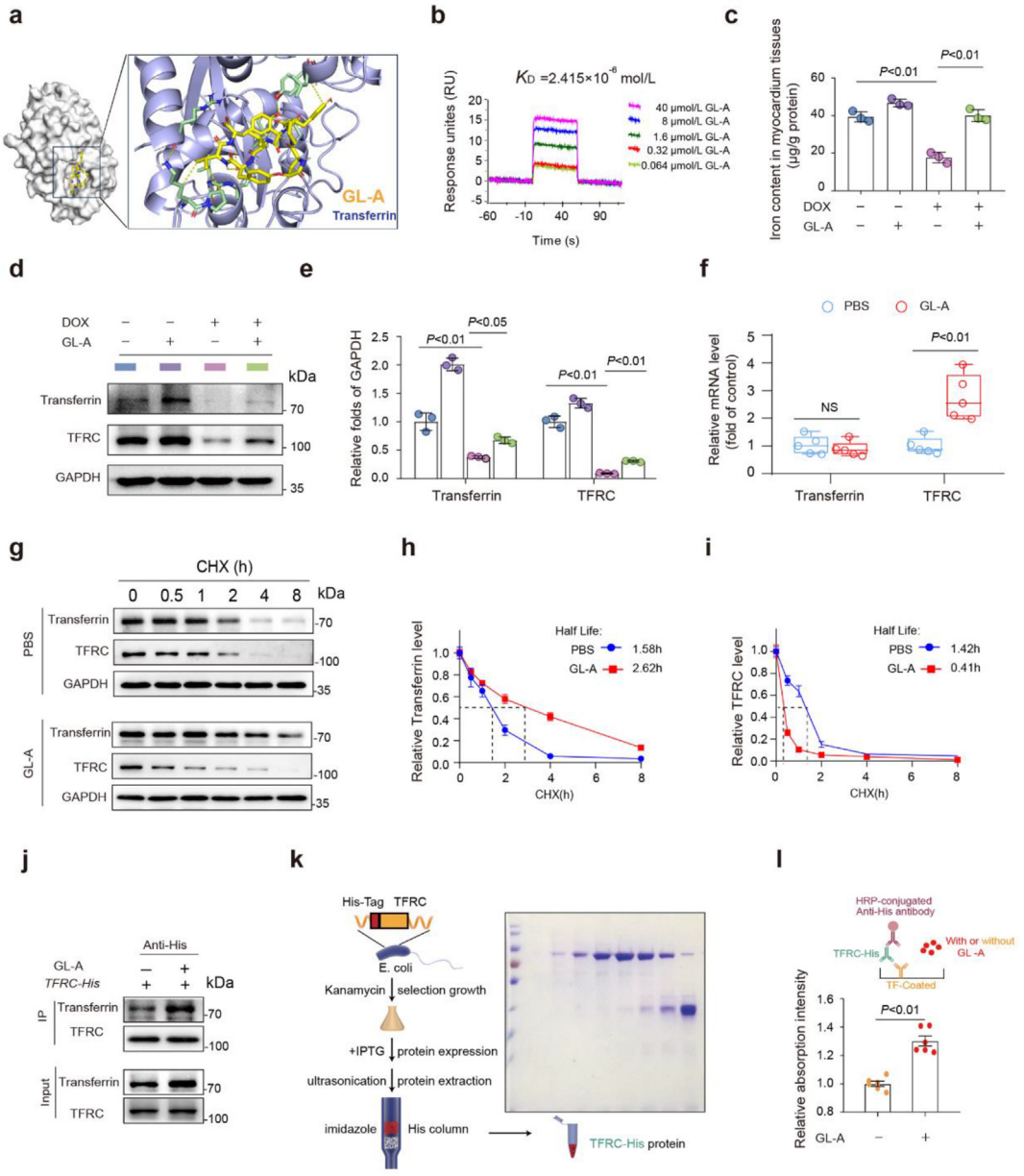

Figure 6 Glycnsisitin A increases the myocardium iron content by enhancing the binding ability of transferrin with TFRC. (a) Molecular docking of transferrin and glycnsisitin A to estimate the binding ability. Images were generated with Discovery Studio. (b) The indicated concentrations of glycnsisitin A were passed over immobilized transferrin on CM5 sensor chips. (c) The iron content in myocardial tissues was assessed by colorimetrically detecting the formation of purple−red compounds resulting from the binding of iron to ferrozine. (d, e) Immunoblotting analysis of the expression levels of transferrin and TFRC in heart tissues: (d) representative immunoblots and (e) the ratio of the indicated protein to GAPDH. (f) Relative mRNA levels of transferrin and TFRC in cardiomyocytes. (g) Analysis of transferrin and TFRC levels after inhibiting protein synthesis with CHX. (h, i) Protein half-life of transferrin and TFRC. (j) Cellular immunoprecipitation with anti-His and blotted with anti-transferrin and anti-TFRC Abs. (k) Schematic illustration depicting the purification process of truncated TFRC-His recombinant proteins expressed in bacteria. The constructed TFRC plasmid with the His-tag was transformed into competent *E. coli*, and IPTG was used to induce recombinant protein production. After being passed through a Ni-NAT column (GE Healthcare), the purification of the target protein TFRC (residues 88−760) was assessed using SDS−PAGE. (l) Schematic illustration demonstrating the ELISA-based method used to verify the affinity between transferrin and TFRC after adding glycnsisitin A. In high-affinity ELISA plates coated with the transferrin protein, TFRC-His was incubated with or without glycnsisitin A, followed by HRP-conjugated anti-his antibody, and then the absorbance at 450 nm was read using a microplate reader. The data are presented as the mean ± SEM.

content in the supernatant, an important marker of cell membrane integrity, was much lower after glycnsisitin A treatment but reversed when TRFC was blocked (Fig. 7c). ATP content analysis revealed that glycnsisitin A treatment noticeably augmented ATP production in cardiomyocytes injured by DOX, which was greatly reduced due to the loss of cellular iron (Fig. 7d). To test the conclusions drawn from primary cardiomyocytes, HF mice were treated with a TFRC neutralizing antibody on Days 13, 16, 19, 22,

and 25 after initial injection of DOX to block TFRC activity (Fig. 7e). We observed that antagonism of TFRC totally eliminated the beneficial effects of glycnsisitin A on cardiac function (Fig. 7f), as evidenced by the reduction in left ventricular EF and FS (Fig. 7g and h), along with a decrease in LV anterior wall thickness and an increase in internal diameter at end-diastole (Fig. 7i and j). Moreover, the inhibition of TRFC markedly diminished both the iron content (Fig. 7k) and ATP levels (Fig. 7l) in the myocardium of mice treated with DOX and glycnsisitin A, which was accompanied by an elevation in serum CK activity (Fig. 7m) and LDH activity (Fig. 7n). Together, these findings suggest the essential and irreplaceable role of TFRC signaling in the mechanism by which glycnsisitin A exerts its cardioprotective activity. By augmenting the binding capacity of transferrin and TFRC, glycnsisitin A preserves myocardial iron homeostasis in the failing heart and notably enhances systolic function, indicating that glycnsisitin A holds promise as a potential candidate for future development of anti-HF drugs.

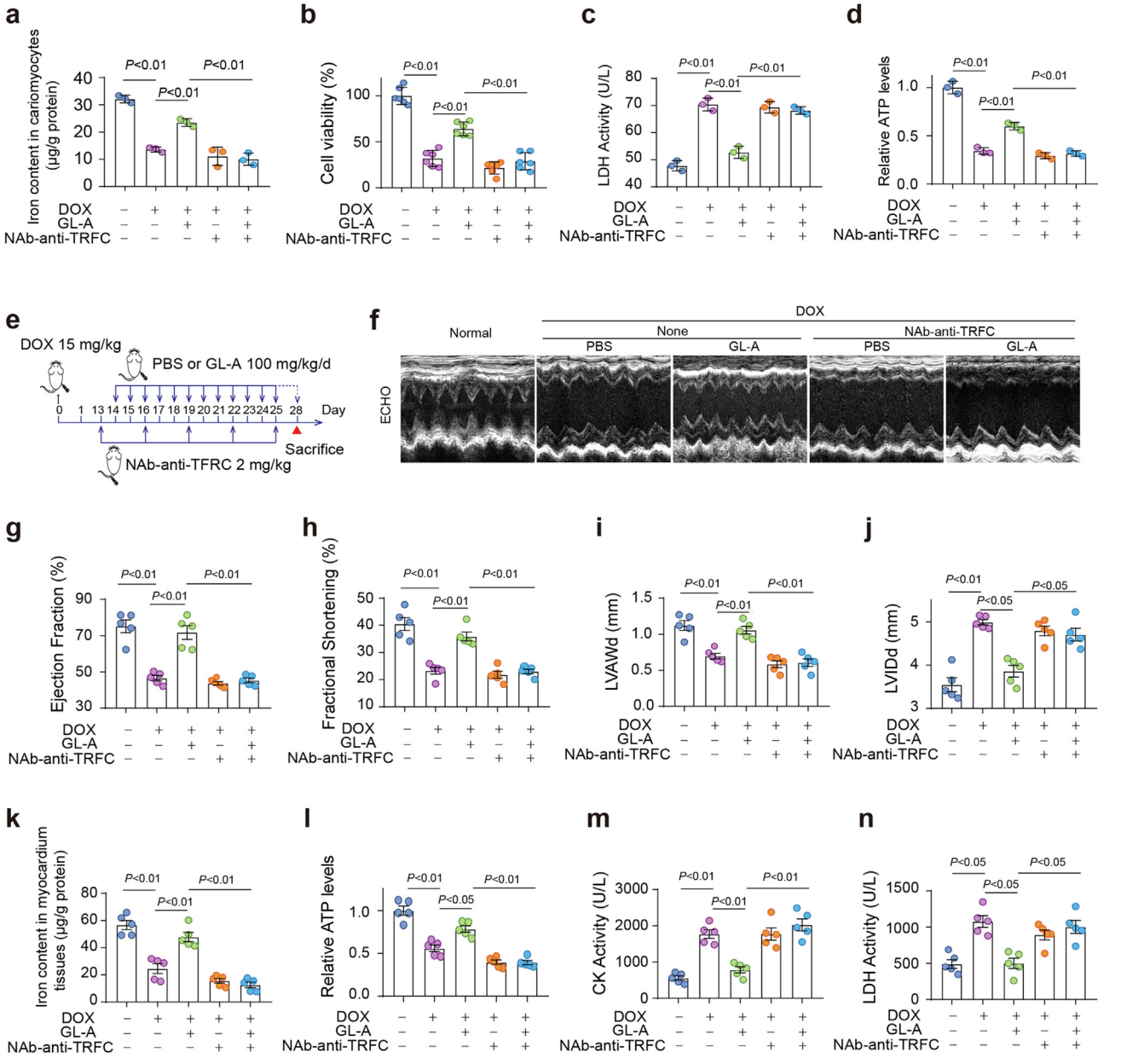

Figure 7 Neutralization of TFRC abolishes the cardioprotective effects of glycnsisitin A. (a) Iron content, (b) cell viability, (c) LDH activity, and (d) relative ATP levels in primary adult rat cardiomyocytes. (e) Schematic illustration of the animal experimental timeline: DOX (15 mg/kg) or PBS (normal) was intraperitoneally injected on Day 0; NAb-anti-TFRC (2 mg/kg) was injected through the tail vein every three days; PBS or glycnsisitin A (100 mg/kg) was administered daily for two weeks by intraperitoneal injection. Mice were sacrificed on Day 28. (f) Representative images of left ventricular M-mode echocardiograms. (g) LV ejection fraction, (h) fractional shortening, (i) End-diastolic left ventricular anterior wall diameter (LVAWd), and (j) internal dimension diameter (LVIDd) were calculated by echocardiographic analysis. (k) Iron content in myocardial tissues. (l) Relative ATP levels, (m) CK activity, and (n) LDH activity in myocardial tissues. The data are presented as the mean ± SEM.

3. Discussion

Currently, the treatment of HF mainly focuses on etiological and surgical treatment. Positive inotropic drugs, diuretics, angiotensin receptor-neprilysin inhibitors (ARNIs), and β receptor blockers are well-established foundational medications used in the treatment of HF[15,16]. However, importantly, while these drugs effectively manage symptoms and slow disease progression, they may not entirely halt the advancement of HF and be suitable for all patients due to their distinct pathological characteristics[17]. Accumulated evidence indicates that HF is usually accompanied by iron deficiency, which in turn can affect the progression and prognosis of various cardiac conditions[18]. Although great progress has been achieved in understanding the mechanism of iron deficiency during HF, finding safe and effective iron supplements or agents to enhance iron absorption for HF therapy remains an unconquered area in drug development[19].

In this study, we identified three novel bicyclic peptides glycnsisitins A−C (**1**−**3**), from the roots of *Glycyrrhiza uralensis*, which exhibited significant cardioprotective effects. Characteristically, they possess unique C−C and C−O−C linkages, leading to greater conformational rigidity and structural stability than conventional peptides[20,21]. In addition, we accurately determined the absolute configuration of glycnsisitin A by single crystal X-ray diffraction using Cu Kα radiation, which establishes a solid foundation for subsequent drug development efforts. Additionally, the biosynthetic pathway for glycnsisitin A was proposed according to the bicycle peptide (legumenin) reported in the reference[14]. First, the precursor peptide was cyclized between the tyrosine and glycine in each core peptide. Then, the N-terminally of the core peptide was cleaved by an endopeptidase. Subsequently, core peptides were N-terminally protected by pyroglutamate formation, through catalysis of glutamine cyclotransferase. Next, the modified core peptide was cyclized between another tyrosine and pyroglutamate. Finally, glycnsisitin A was produced by C-terminal proteolysis (Fig. 8). Due to the proposed biosynthetic pathway not being verified by experiments, there still exist other possible pathways. Pharmacological studies have demonstrated that glycnsisitin A can effectively alleviate DOX-induced HF by increasing iron uptake in cardiomyocytes and restoring iron content to a normal level. We not only reveal a previously unidentified cardioprotective mechanism for licorice but also propose an attractive therapeutic candidate for treating HF in individuals with iron deficiency.

Reportedly, enhancing erythropoiesis to correct anemia does not provide beneficial effects to patients with HF[22], while intravenous iron supplementation has been shown to improve the quality of life in these patients[23], suggesting that the relative deficiency of iron in nonerythrocytic tissues may play an important role in the pathophysiological mechanism of HF[24]. Indeed, our study confirms the presence of abnormal iron metabolism in hearts and cardiomyocytes injured by DOX, as observed by the reduction in iron content and decreased levels of both transferrin and TFRC, which are responsible for facilitating iron transport and uptake. Our findings indicate that peptides or small molecules that specifically enhance the affinity of transferrin and TFRC, thereby improving iron uptake in cardiomyocytes, could offer a novel therapeutic option for the treatment of HF.

Under pathological conditions, mitochondria serve as the main origin of reactive oxygen species (ROS) in the heart, and excessive generation of mitochondrial ROS leads to accumulation of mitochondrial superoxide and reduction of ATP[25,26]. In addition, Melenovsky et al. observed that iron deficiency-induced mitochondrial dysfunction can also impair cellular energy supplement and cardiac function[27]. The clinical use of DOX is significantly hindered by its dose-dependent cardiotoxicity, leading to subsequent HF. This cardiotoxicity is characterized by excessive production of ROS and impaired cardiac energy metabolism[28]. Currently, dexrazoxane (DXZ) is the exclusive FDA-approved drug for DOX-induced HF. However, its clinical application is constrained by its potential to confer chemotherapy resistance to cancer cells[29]. Although we did not specifically investigate the potential of glycnsisitin A as a useful candidate for adjuvant chemotherapy in DOX treatment, exploring this possibility may offer valuable insights and is worth further investigation.

TFRC is a membrane-bound protein that plays a vital role in maintaining intracellular iron homeostasis. The binding of iron-carried transferrin with TFRC on the cell membrane typically initiates the endocytosis of the TFRC-transferrin complex, thereby accelerating cellular iron uptake and enclosure within endosomes. If necessary, iron is transported across the endosomal membrane by DMT1, located on the membrane of the endosome.

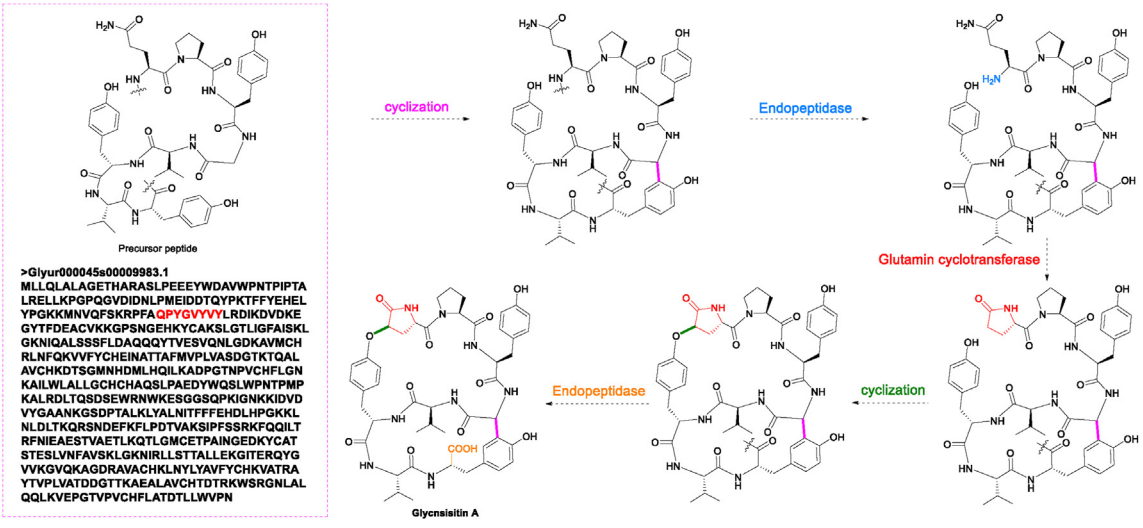

Figure 8 Proposed biosynthetic pathway of glycnsisitin A.

Subsequently, it is released into the cytoplasm, where it can participate in a variety of cellular processes[30]. The mice lacking the TFRC gene died during the second week following birth, exhibiting cardiac enlargement, compromised cardiac function, impaired mitochondrial respiration, and inhibited mitophagy[31]. In our current investigation, we observed a decline in the protein expression of transferrin and TFRC in HF tissue. However, following the administration of glycnsisitin A, there was an increase in the levels of transferrin and TFRC, which may be attributed to the restoration of mRNA levels or the facilitation of transcription and translation processes. Additionally, glycnsisitin A enhanced the interaction between transferrin and TFRC, resulting in the promotion of cellular iron uptake and restoration of intracellular iron levels to normal, thus improving mitochondrial energy metabolism and restoring cardiac function. Nevertheless, the precise molecular mechanism by which glycnsisitin A restores mitochondrial function following the restoration of iron homeostasis requires additional investigation.

4. Conclusions

In summary, three novel bicyclic peptides that exhibited noteworthy cardioprotective properties were isolated from the roots of *Glycyrrhiza uralensis*. In comparison to glycnsisitin B and C, glycnsisitin A demonstrates the most efficacious cardiomyocyte protection against doxorubicin (DOX)-induced injury. Both the findings from *in vitro* experiments using primary cultured cardiomyocytes and data obtained from *in vivo* heart failure animal models corroborate that the principal mechanism responsible for the anti-heart failure (HF) pharmacological activity of glycnsisitin A attributed to its capacity to modulate intracellular iron uptake through the transferrin−transferrin receptor (TF-TFRC) pathway. This investigation furnishes valuable insights into the development of cardiotonic therapeutic strategies predicated on the regulation of myocardial iron homeostasis, with glycnsisitin A emerging as a promising candidate warranting further exploration and development.

5. Experimental

5.1. General experimental procedure

The optical rotations and UV spectra were recorded with JASCO P-2000 and V650 spectrometers (JASCO, Easton, MD, USA), respectively. The infrared spectra were recorded on a Nicolet 5700 spectrometer (Thermo Scientific, Waltham, MA, USA). The NMR spectra were recorded with Varian 500 MHz (Varian, Inc., Palo Alto, CA, USA) and Bruker 600 MHz NMR spectrometers (Bruker-Biospin, Billerica, MA, USA). HRESIMS reports were obtained from Q Exactive Focus LC−MS/MS system (Thermo Scientific, MA, USA). ESIMS reports were obtained from UPLC H-Class/SQ Detector 2 system (Waters, MA, USA). Preparative HPLC was performed using a Shimadzu LC-6AD instrument with an SPD-10A detector (Shimadzu Corp., Tokyo, Japan), using a YMC-Pack ODS-A column (250 mm × 20 mm, 5 μm; YMC Corp., Kyoto, Japan). HPLC-DAD analysis was performed using an Agilent 1260 series system with an Apollo C_{18} column (250 mm × 4.6 mm, 5 μm). Column chromatography was performed on macroporous resin HP-20 (Diaion, Japan), RP-C_{18} (50 μm, YMC Corp.), and Sephadex LH-20 (Pharmacia Fine Chemicals, Uppsala, Sweden). X-ray diffraction intensity data were obtained on a Bruker APEX-II CCD single-crystal diffractometer using Cu Kα radiation.

Crystallographic data (CCDC 2254397) for Glycnsisitin A (**1**). Empirical formula: $C_{59}H_{100}N_8O_{24}$, orthorhombic, crystal size = 0.23 × 0.22 × 0.20 mm^3, space group = $P2_12_12_1$; unit cell dimensions: a = 10.4512(5) Å, b = 18.9655(8) Å, c = 35.9881(14) Å, V = 7133.3(5) $Å^3$, ρ_{calcd} = 1.216 g/cm^3, Z = 4, T = 150.00 K, μ (Cu Kα) = 0.788 mm^{-1}, a total of 36,959 reflections were collected ($6.772^\circ \leq 2\theta \leq 149.506^\circ$) with 14149 independent reflections (R_{int} = 0.0500, R_{sigma} = 0.0570). Parameters = 862 and restraints = 4. Final R indexes [$I \geq 2\sigma(I)$]: R_1 = 0.0949, wR_2 = 0.2514. Final R indexes [all data]: R_1 = 0.1003, wR_2 = 0.2616. Largest difference peak and hole = 0.57 and −0.45 e $Å^{-3}$. Flack parameter = 0.00(9).

5.2. Plant material

The roots of *Glycyrrhiza uralensis* were purchased from Bozhou City, Anhui Province, PRC in April 2019 and identified by Professor Lin Ma. A voucher specimen (ID number: ID-S-2592) was deposited at the Institute of Materia Medica, Peking Union Medical College and Chinese Academy of Medical Sciences, Beijing, China.

5.3. Extraction and isolation

The roots of *Glycyrrhiza uralensis* (200.0 kg) were exhaustively extracted with 80% ethanol (2 × 1000 L) under reflux conditions. The ethanol was evaporated by reduced pressure, and then, another 80 L water was added to the remaining solvent (120 L). The treated solvent was then subjected to a 24-h standing under 4 °C. The liquid supernatant was reserved and condensed under reduced pressure to afford a brown concentrated solution, followed by the first macroporous resin (Diaion HP-20) chromatography column elution, and eluted with H_2O, 15% ethanol, 50% ethanol, and 95% ethanol. The liquid supernatant of 50% ethanol was reserved and condensed under reduced pressure, followed by Sephadex LH-20 chromatography column elution, and eluted with water to afford six subfractions (Fractions A1 to A6). The bicyclic peptides were found in subfractions Fra. A3 (109 g) according to the HPLC and HRMS analyses. Then, Fra. A3 was chromatographed over a RP-C_{18} column by eluting with H_2O/MeOH (from 80:20 to 70:30, 0.05% CH_3COOH) to give 64 subfractions. Among them, there was colorless crystal precipitation in subfractions 22−35 to give compound **1** (30.0 g). The rest of the subfractions 22−35 were further purified by preparative HPLC (MeCN/H_2O, 21:79, *v*/*v*, HOAc, 0.1%) to give compounds **2** (20.3 mg) and **3** (8.5 mg).

5.4. Structure characterization

Glycnsisitin A (**1**): Colorless crystal; UV λ_{max} (MeOH) (logε): 203 (4.86), 223 (4.45), 280 (3.76) nm (Supporting Information Fig. S9); $[\alpha]_D^{20}$ +49 (*c* 0.1 MeOH); HRESIMS *m*/*z* 967.4191 $[M + H]^+$ (calcd 967.4196) (Supporting Information Fig. S7); IR ν_{max}: 3302, 2965, 1659, 1513, 1447, 1267, 1236, 1048, 826 cm^{-1} (Supporting Information Fig. S8); ^1H NMR and ^{13}C NMR data see Supporting Information Tables S1 and S2.

Glycnsisitin B (**2**): White amorphous powder; UV λ_{max} (MeOH) (logε): 203 (4.74), 219 (4.45), 279 (3.60) nm (Supporting Information Fig. S18); $[\alpha]_D^{20}$ +37 (*c* 0.1 MeOH);

HRESIMS *m/z* 967.4192 $[M + H]^+$ (calcd 967.4196) (Supporting Information Fig. S16); IR ν_{max}: 3385, 2964, 1659, 1514, 1445, 1267, 1228, 1105, 1031 cm^{-1} (Supporting Information Fig. S17); ^1H NMR and ^{13}C NMR data see Tables S1 and S2.

Glycnsisitin C (**3**): White amorphous powder; UV λ_{max} (MeOH) (logε): 203 (4.81), 226 (4.27), 282 (3.70) nm (Supporting Information Fig. S27); $[\alpha]_D^{20}$ +30 (*c* 0.1 MeOH); HRESIMS *m/z* 983.4139 $[M + H]^+$ (calcd 983.4145) (Supporting Information Fig. S25); IR ν_{max}: 3302, 2966, 1659, 1512, 1446, 1266, 1223, 1117, 824 cm^{-1} (Supporting Information Fig. S26); ^1H NMR and ^{13}C NMR data see Tables S1 and S2.

5.5. Molecular docking and SPR assay

The crystallographic structures of transferrin (PDB: 1D3K) and TFRC (PDB: 3S9N) were downloaded from the Protein Data Bank (http://www.rcsb.org/pdb/). The energy of each compound was minimized to its local minima using an MMF94X force field. The protein was held rigid in the docking process and the compound was flexible. Blind docking was carried out with AutoDock Vina (http://vina.scripps.edu/)[32]. The initial grid box size was 15.0 Å × 15.0 Å × 15.0 Å in the *x*, *y*, and *z* dimensions. The grid box center was put on $x = 36.8$, $y = -63.0$, and $z = 53.4$ with the protein positioned at the center of the box. The docking results were analyzed with AutoDockTools using the cluster analysis tool PyMOL (https://www.pymol.org).

SPR assays were performed on a Biacore T100 instrument. The transferrin was immobilized on CM5 chips by amino coupling under the catalyzation of *N*-hydroxysuccinimide (NHS). Then the response units were recorded when different concentrations of glycnsisitin A flowed through the chip. The dissociation constant (K_D) was calculated according to the Bia-evaluation software.

5.6. Primary adult rat cardiomyocyte isolation and culture

Primary adult rat cardiomyocytes were isolated from male Sprague−Dawley rats (about 280 g) through an optimized Langendorff perfusion system. The SD rat was anesthetized with an intraperitoneal injection of 350 mg/kg avertin (Sigma, T48402), and after pinching the toes without reaction, sufficient alcohol was sprayed on the rat's abdomen. The abdominal skin was cut open and heparin (Solarbio, H8060, 100 IU in 1 mL saline) was injected into the inferior vena cava. The sternum was cut open, the aortic arch was cut off and the heart was separated in a plate containing KHB buffer (118 mmol/L NaCl, 4.8 mmol/L KCl, 25 mmol/L HEPES, 0.6 mmol/L KH_2PO_4, 1.25 mmol/L $MgSO_4$, 11 mmol/L glucose, 5 mmol/L Taurine, 10 mmol/L BDM, pH = 7.35−7.55, 37 °C and sterile filtered) to remove excess tissue and trachea. After perfusing the heart with solution E [1 mg/mL BSA (Sigma, V900933), 0.7 mg/mL collagenase II (Worthington, LS004176), 0.2 mg/mL hyaluronidase (Sigma, H3506) and 25 mmol/L $CaCl_2$] for 10 min, 12.5 μL of 0.1 mol/L $CaCl_2$ solution was added, 5 min later, extra 25 μL 0.1 mol/L $CaCl_2$ was added for the next 15 min digestion. The heart was removed and placed in a dish with solution E, gently torn with tweezers, and filtered through a 75 μm cell strainer. The cardiomyocytes were purified by three times of gravity sedimentation and cultured with M199 medium (Gibco9, 218712) containing 10% fetal bovine serum (Biological Industries, BI199), 100 U/mL Penicillin−Streptomycin (Livinen, LVN1007) and 1% glutamine (Gibco, 35050-061) in Laminin-coated (Gibco, 23017-015) plates.

5.7. Cell viability assay

Rat myocardial H9C2 cell was purchased from national biomedical medical cell resource (BMCR) which is cultured in Dulbecco's modified eagle media (DMEM, Sigma, D6429) supplemented with 10% fetal bovine serum and 100 U/mL penicillin-streptomycin in 5% CO_2, 37 °C. H9C2 was seeded at 5000 cells/well/100 μL complete medium in 96-well black-sided plates with clear bottoms (Labselect, 11514) and cultured overnight. Then, H9C2 cells were treated with 8.6 μmol/L Doxorubicin (DOX) and indicated compounds. After 12 h incubation, discarded the supernatant and replaced it with a complete medium containing 10% alamar blue assay (Solarbio, A7631) for another 4 h reaction. After the medium changed from non-fluorescent blue to fluorescent pink, fluorescence values (IF) were detected on a microplate reader with excitation at 530 nm and emission at 590 nm. The cell viability rate was calculated as Eq. (1):

$$\text{Viability rate } (\%) = [(IF_A - IF_0)/(IF_B - IF_0)] \times 100 \quad (1)$$

where IF_A represents the IF value of compounds treated cells; IF_B represents the IF value of control cells; and IF_0 represents the IF value of the medium.

5.8. LDH and ATP assay

We collected the cells and supernatant treated with or without DOX and Glycnsisitin A for 12 h and measured them using the LDH activity Kit (Solarbio, BC0685) and ATP Assay Kit (Byotime, S002) according to the manufacturer's instructions.

5.9. Mitochondrial superoxide detecting

Isolated primary rat cardiomyocytes were seeded in glass-bottomed confocal dishes and incubated with 10 μmol/L glycnsisitin A and/or 8.6 μmol/L DOX for 6 h, and MitoSox™ Red (Thermo Fisher, M36008) was prepared as stock solution and working solution according to the manufacturer's instructions. Then incubate cells for 30 min at 37 °C and 5% CO_2, protecting from light and washing cells gently 3 times with warm buffer (HBSS with calcium and magnesium). At last, view the cell's spectral properties which absorb and emit optimally at 396 and 610 nm through laser confocal microscopy.

5.10. Animal experiments

All animal studies were approved by the Animal Experimentation Ethics Committee of the Chinese Academy of Medical Sciences (ethics number: 00003623), and all procedures were conducted following the guidelines of the Institutional Animal Care and Use Committees of the Chinese Academy of Medical Sciences.

We used doxorubicin to induce the acute HF in ICR mice. The ICR mice (male, about 40 g, 10-week-old, SPF grade, Sipeifu) were administered with PBS in the normal group and the remaining groups received a single intraperitoneal high-dose of DOX (15 mg/kg). The mouse model of acute HF was successfully prepared on Day 14. Then, the DOX-treated ICR mice were randomized into 5 groups: DOX model group, glycnsisitin A low dose (50 mg/kg) group, glycnsisitin A medium dose (100 mg/kg) group, glycnsisitin A high dose (200 mg/kg) group, and positive drug (cedilanid 150 μg/kg) group. Glycnsisitin A (low, medium, high dose) or positive drug cedilanid was administered

intraperitoneally daily on Days 15−28 after DOX administration. Meanwhile, normal and model groups were injected intraperitoneally with the same volume of PBS (10 mL/kg). In the following animal experiment of neutralization of TFRC, mice were randomly assigned to experimental groups: normal group, DOX model group, glycnsisitin A (100 mg/kg) treatment group, NAb-anti-TFRC (2 mg/kg) group, and glycnsisitin A + NAb-anti-TFRC group. Glycnsisitin A (100 mg/kg) or the same volume of PBS was given daily by intraperitoneal injection on Days 14−28 after the initial injection of DOX. Meanwhile, NAb-anti-TFRC was injected through the tail vein on Days 13, 16, 19, 22, and 25 after DOX administration to block TFRC activity.

Mice's heart structure and function were detected by the echocardiography detection system at 8 h after drug administration on Day 28, and heart tissue and serum were collected at 8 h after drug administration on Day 29. Mouse hearts were fixed with 4% paraformaldehyde (Bioss, C0106002), and Hematoxylin and eosin (H&E) or Sirius red was used to strain the cardiac tissue sections according to standard protocols. Mice blood was collected and centrifuged at 4500 rpm for 15 min at 4 °C to obtain serum. The CK, LDH activity, BNP (Solarbio, SEKM-0151), and NT-proBNP (Solarbio, SEKM-0298) content of mice serum were used to evaluate the myocardial injury. The deaths of the animals were recorded daily.

5.11. Detection of cardiac function

Mice were anesthetized by intraperitoneal injection of avertin and the chest was depilated. Then, they were fixed on the 37 °C thermostatic operation table and tested using the VisualSonics Vevo770 ultrasound system. First, a 10 MHz ultrasound probe was used to monitor the long-axis direction of the mouse heart. After determining the position of the left ventricular papillary muscle, it was transferred to the short-axis direction of the heart for monitoring, and the M-type ultrasound pattern of 10−20 cardiac cycles was recorded. The Vevo 770 software was used to calculate the ejection fraction (EF), fractional shortening (FS), left ventricular anterior wall diameter (LVAWd), and left ventricular internal dimension diameter (LVIDd) to evaluate cardiac function.

5.12. RNA sequencing (RNA-Seq) analysis

Three samples from each group were sent to Orvisen Gene Technology Ltd. (Beijing) for the extraction and purification of the total RNA, preparation of RNA Library, and sequenced on the second-generation high-throughput Illumina platform. Differentially expressed genes (DEGs) were analyzed and KEGG signaling pathway analysis and Gene set enrichment analysis (GSEA) were performed.

5.13. Iron content determination

Iron content of cardiomyocytes or tissues was measured by colorimetric assay using the properties of purple compounds generated by combining iron to ferrozines with a Total Iron Content Colorimetric Assay Kit (Applygen, E1042). After the animal experiment, a little mouse heart tissue was cut into lysate, and ground into homogenate. The cells were evenly spread into a six-well plate. After the stimulation, the media was discarded, and washed twice with PBS, 200 μL of lysate was added to lyse the cells and put on a shaker at room temperature for 2 h. 3 mmol/L of the standard solution was diluted to 300, 150, 75, 37.5, 18.75, 9.38, 4.69 μmol/L. Mix the stock buffer with 4.5% potassium permanganate solution at 1:1, which is called solution A. Then, 100 μL sample or standard solution was transferred to a 1.5-mL centrifuge tube, mixed with 100 μL of solution A, and incubated at 60 °C for 1 h. After 1 h, the solution was cooled to room temperature. 30 μL of iron ion-detection reagent was added, mixed, and incubated at room temperature for 30 min. 200 μL solution was taken into 96-well plates and the absorbance at 550 nm was determined. Standard curves were plotted and the iron ion concentration of samples was calculated.

5.14. Protein purification

TFRC-His recombinant proteins were purified by Ni-NAT affinity chromatography. TFRC plasmid was constructed by GeneCopoeia. In order to successfully express target transmembrane protein from the prokaryotic system, we deleted the N-terminal transmembrane region of TFRC while leaving the C-terminal transferrin-binding region (position 569−760) completely intact. Thus, the truncated TFRC sequence (position 88−760) was amplified by PCR and verified by DNA gel. The PET28A was digested overnight with Nhe I and EcoR I at 37 °C. The digestion effect was verified by DNA gel analysis. The 5-kb digestion product was recovered from the gel to prepare into a linearized vector plasmid and the target fragment was linked with the vector. Adding 8 μL of linearized plasmid, 6.6 μL of fragment, 4 μL of buffer, and 2 μL of enzyme to a microcentrifuge tube, after incubation at 37 °C for 30 min, the recombinant plasmid was transformed into DH-5α competent cells and seeded on the Kana Luria−Bertani (LB) solid medium. The plates were incubated in a 37 °C incubator for colony amplification. Three colonies were randomly picked, purified, and sequenced. The sequencing results were compared by blast, and the verified colony was amplified in order to obtain sufficient plasmid DNA for further experiments. The aforementioned TRFC-His plasmid was transformed into transetta (DE 3) competent cells. After preculture in Kana solid medium, fresh bacterial colonies were transferred to a liquid medium and cultivated at 37 °C for 24 h then diluted 200 times with LB media. Meanwhile, monitor the absorbance of LB media at 600 nm, When OD_{600} reached 0.6, isopropyl β-D-thiogalactoside (IPTG) was added in a final concentration of 1.0 mmol/L to induce TRFC synthesis. After incubating for 4 h at 17 °C, the overexpression efficiency was verified by SDS-PAGE analysis of the induced and noninduced cells' total protein extracts. The TRFC-contained bacteria were collected, sonicated, and centrifuged at 12,000 rpm for 10 min and the supernatant was used for subsequent purification. Before loading the sample, 100 mL PBS was used to wash the pump and Ni-NTA column (GE Healthcare). Then, the supernatants were slowly loaded into the column and 300 mmol/L imidazole solution (formulated in PBS, protease inhibitor cocktail added, passed through a 0.22 μm filter membrane) was used as mobile phase for the purification. Fractions were collected and denatured with 5× SDS loading buffer, then analyzed by SDS-PAGE and subsequent Coomassie blue staining. Finally, the corresponding tubes with a single band (84-kDa) were collected and concentrated using 50-kDa filter tubes (Millipore).

5.15. ELISA-based affinity detection

Transferrin proteins were dissolved with ELISA coating buffer (Sigma−Aldrich, C3041), and 100 μL of 1 mg/mL transferrin protein solution was added to the ELISA plates in each well. The plate was sealed against volatilization and incubated overnight at 4 °C. After discarding the transferrin solution and three washes in

PBST, 200 μL of blocking solution was added to avoid the nonspecific binding. After 1 h incubation at room temperature, discard the blocking solution, and 100 μL of 1 mg/mL TFRC protein diluted with blocking solution was added to each well, with or without 10 μmol/L glycnsisitin A, incubated overnight at 4 °C. Because the purified TFRC protein had His tag, anti-His antibody, and HRP-conjunct secondary antibody were incubated for the next TMB chromogenic reaction.

5.16. *Statistical analysis*

The experimental results are expressed by mean ± standard error of the mean (mean ± SEM). First, Normality and Lognormality Tests were used to test whether the data conform to the normal distribution and One-way ANOVA followed. If the variances were homogeneous ($P > 0.05$), data was tested by Ordinary ANOVA test. If the variances were different ($P \leq 0.05$), data was tested by non-parametric Brown-Forsythe and Welch ANOVA test. Statistics of the pathological grading data are performed using the chi-square test. The survival rate is compared using the Kaplan−Meier analyses. Statistical difference was considered at $P < 0.05$ and considered significant at $P < 0.01$.

Acknowledgments

We would be grateful to Yuanyuan Chen, Bingxue Zhou, and Zhenwei Yang (Institute of Biophysics, Chinese Academy of Science) for the technical help with Biacore experiments. This work was supported by Chinese Academy of Medical Sciences (CAMS) Innovation Fund for Medical Sciences (2022-I2M-2-002, 2021-I2M-1-016, and 2022-I2M-1-014, China), the Beijing Outstanding Young Scientist Program (BJJWZYJH01 201910023028, China), Chinese Academy of Medical Sciences (CAMS) Central Public-interest Scientific Institution Basal Research Fund (2018PT35004, Molecular Mechanism and Target Discovery of Metabolic Disorder and Tumorigenesis, CAMS Key Laboratory).

Author contributions

Yanan Yang, Xiaowei Zhang, and Peicheng Zhang initiated and supervised the project. Ziming Feng, Jianshuang Jiang, and Xiang Yuan performed the extraction experiments. Meng Yuan, Yuanyuan Liu, Xu Zhang, and Lingfeng Qin designed and performed the isolation experiments. Meng Yuan, Yuanyuan Liu, Xu Zhang, Lingfeng Qin, Yanan Yang, and Peicheng Zhang elucidated the structures of compounds **1**−**3**. Jichao Zhou, Xiaoli Wei, Ruibing Xu, Zhimeng Zhang, Bing Cui, Pingping Li, and Xiaowei Zhang designed and performed biological experiments. Jichao Zhou, Xu Zhang, Xiaoli Wei, and Meng Yuan contributed to the writing of this manuscript.

Conflicts of interest

The authors declare no conflicts of interest.

Appendix A. Supporting information

Supporting information to this article can be found online at https://doi.org/10.1016/j.apsb.2024.02.026.

References

1. Heidenreich PA, Bozkurt B, Aguilar D, Allen LA, Byun JJ, Colvin MM, et al. 2022 AHA/ACC/HFSA Guideline for the management of heart failure: executive summary: a report of the American college of cardiology/American heart association joint committee on clinical practice guidelines. *Circulation* 2022;**145**:e876−94.
2. Zannad F. Rising incidence of heart failure demands action. *Lancet* 2017;**391**:518−9.
3. Mcdonagh TA, Metra M, Adamo M, Gardner RS, Baumbach A, Böhm M, et al. 2021 ESC Guidelines for the diagnosis and treatment of acute and chronic heart failure: developed by the task force for the diagnosis and treatment of acute and chronic heart failure of the European society of cardiology (ESC). With the special contribution of the heart failure association (HFA) of the ESC. *Eur J Heart Fail* 2022;**24**:4−131.
4. He X, Du TL, Long TX, Liao XX, Dong YG, Huang ZP. Signaling cascades in the failing heart and emerging therapeutic strategies. *Signal Transduct Tar* 2022;**7**:134.
5. Pasricha SR, Tye-Din J, Muckenthaler MU, Swinkels DW. Iron deficiency. *Lancet* 2021;**391**:233−48.
6. Savarese G, Haehling SV, Butler J, Cleland JG, Ponikowski P, Anker SD. Iron deficiency and cardiovascular disease. *Eur Heart J* 2023;**44**:14−27.
7. Rohr M, Brandenburg V, Rocca HB. How to diagnose iron deficiency in chronic disease: a review of current methods and potential marker for the outcome. *Eur J Med Res* 2023;**28**:15.
8. Kalra PR, Cleland JGF, Petrie MC, Thomson EA, Kalra PA, Squire LB, et al. Intravenous ferric derisomaltose in patients with heart failure and iron deficiency in the UK (IRONMAN): an investigator-initiated, prospective, randomised, open-label, blinded-endpoint trial. *Lancet* 2022;**400**:2199−209.
9. Lerman JB, Newby LK. In HF with iron deficiency, IV ferric derisomaltose was associated with lower rates of HF hospitalization or CV death. *Ann Intern Med* 2023;**176**:JC40.
10. Hu MT, Li HR, Ni SK, Wang SF. The protective effects of Zhi-Gan-Cao-Tang against diabetic myocardial infarction injury and identification of its effective constituents. *J Ethnopharmacol* 2023;**309**:116320.
11. Ji S, Li ZW, Song W, Wang YR, Liang WF, Li K, et al. Bioactive constituents of *Glycyrrhiza uralensis* (Licorice): discovery of the effective components of a traditional herbal medicine. *J Nat Prod* 2016;**79**:281−92.
12. Kao TC, Wu CH, Yen GC. Bioactivity and potential health benefits of licorice. *J Agric Food Chem* 2014;**62**:542−53.
13. Shang ZP, Liu CR, Qiao X, Ye M. Chemical analysis of the Chinese herbal medicine licorice (Gan-Cao): an update review. *J Ethnopharmacol* 2022;**299**:115686.
14. Chigumba DN, Mydy LS, Waal FD, Li WJ, Shafiq K, Wotring JW, et al. Discovery and biosynthesis of cyclic plant peptides *via* autocatalytic cyclases. *Nat Chem Biol* 2022;**18**:18−28.
15. Maack C, Eschenhagen T, Hamdani N, Heinzel FR, Lyon AR, Manstein DJ, et al. Treatments targeting inotropy. *Eur Heart J* 2019;**40**:3626−44.
16. Rossignol P, Hernandez AF, Solomon SD, Zannad F. Heart failure drug treatment. *Lancet* 2019;**393**:1034−44.
17. Goyal P, Mangal S, Krishnaswami A, Rich MW. Polypharmacy in heart failure: progress but also problem. *Am J Med* 2021;**134**:1071−3.
18. Loncar G, Obradovic D, Thiele H, Haehling SV, Lainscak M. Iron deficiency in heart failure. *ESC Heart Fail* 2021;**8**:2368−79.
19. Anand IS, Gupta P. Anemia and iron deficiency in heart failure: current concepts and emerging therapies. *Circulation* 2018;**138**:80−98.
20. Tan NH, Zhou J. Plant cyclopeptides. *Chem Rev* 2006;**106**:840−95.
21. Rhodes CA, Pei DH. Bicyclic peptides as next-generation therapeutics. *Chem Eur J* 2017;**23**:12690−703.
22. Bolger AP, Bartlett FR, Penston HS, O'Leary J, Pollock N, Kaprielian R, et al. Intravenous iron alone for the treatment of anemia in patients with chronic heart failure. *J Am Coll Cardiol* 2006;**48**:1225−7.

23. López-vilella R, Lozano-edo S, Martín PA, Jover-pastor P, Ezzitouny M, Romero JS, et al. Impact of intravenous ferric carboxymaltose on heart failure with preserved and reduced ejection fraction. *ESC Heart Fail* 2022;**9**:133−45.
24. Ponikowski P, Veldhuisen DJV, Comin-colet J, Ertl G, Komajda M, Mareev V, et al. Beneficial effects of long-term intravenous iron therapy with ferric carboxymaltose in patients with symptomatic heart failure and iron deficiency. *Eur Heart J* 2015;**36**:657−68.
25. Federico M, Fuente SDL, Palomeque J, Sheu SS. The role of mitochondria in metabolic disease: a special emphasis on heart dysfunction. *J Physiol* 2021;**599**:3477−93.
26. He YN, Huang W, Zhang C, Chen LM, Xu RC, Li N, et al. Energy metabolism disorders and potential therapeutic drugs in heart failure. *Acta Pharm Sin B* 2021;**11**:1098−116.
27. Melenovsky V, Petrak J, Mracek T, Benes J, Borlaug BA, Nuskova H, et al. Myocardial iron content and mitochondrial function in human heart failure: a direct tissue analysis. *Eur J Heart Fail* 2017;**19**:522−30.
28. Mitry MA, Edwards JG. Doxorubicin induced heart failure: phenotype and molecular mechanisms. *Int J Cardiol Heart Vasc* 2016;**10**:17−24.
29. Chen Y, Shi SX, Dai Y. Research progress of therapeutic drugs for doxorubicin-induced cardiomyopathy. *Biomed Pharmacother* 2022;**156**:113903.
30. Moharir SC, Sirohi K, Swarup G. Regulation of transferrin receptor trafficking by optineurin and its disease-associated mutants. *Prog Mol Biol Transl Sci* 2023;**194**:67−78.
31. Xu WJ, Barrientos T, Mao L, Rockman HA, Sauve AA, Andrews NC. Lethal cardiomyopathy in mice lacking transferrin receptor in the heart. *Cell Rep* 2015;**13**:533−45.
32. Trott O, Olson AJ. AutoDock Vina: improving the speed and accuracy of docking with a new scoring function, efficient optimization, and multithreading. *J Comput Chem* 2010;**31**:455−61.